# Rational synthesis of CoFeP@nickel-manganese sulfide core-shell nanoarrays for hybrid supercapacitor

Yameng Wang[a,b], Yan Zhang[b], Cheng Du[b], Jian Chen[b], Zhengfang Tian[a,b], Mingjiang Xie[a,b], Liu Wan*[a,b]

[a]College of Materials and Chemical Engineering, China Three Gorges University, Yichang, 443002, China

[b]Hubei Key Lab for Processing and Application of Catalytic Materials, College of Chemical Engineering, Huanggang Normal University, Huanggang, 438000, China

*Corresponding author.

E-mail: wanliuok2006@163.com

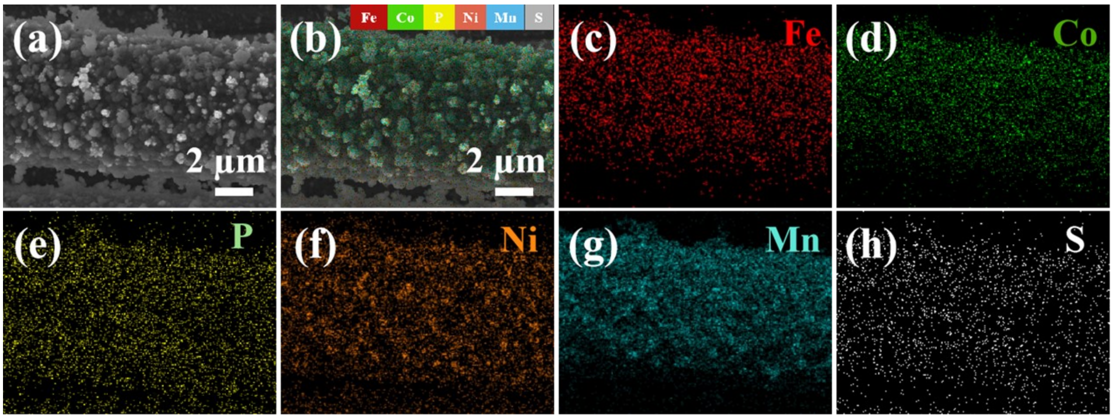


Fig. S1 (a,b) SEM images for the corresponding EDX mapping image of CoFeP@NiMnS/CC, (c) Fe elemental mapping, (d) Co elemental mapping, (e) P elemental mapping, (f) Ni elemental mapping, (g) Mn elemental mapping, and (h) S elemental mapping.

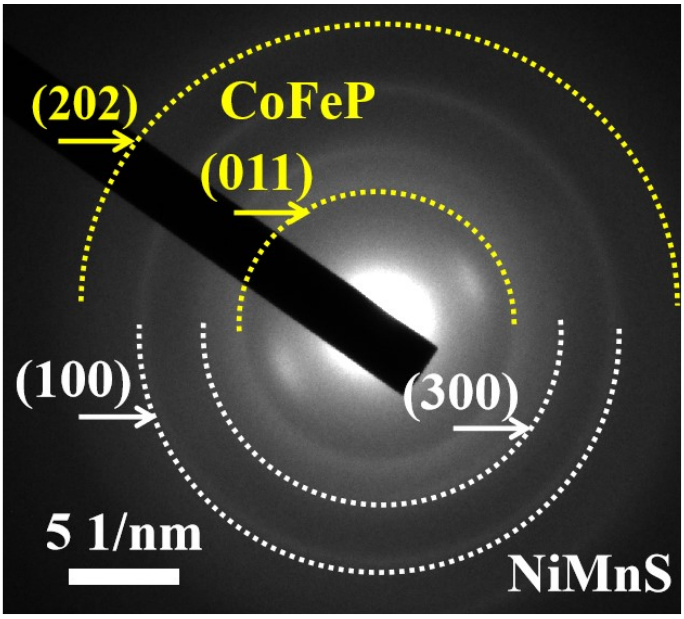


Fig. S2 The selected area electron diffraction (SEAD) pattern of CoFeP@NiMnS.

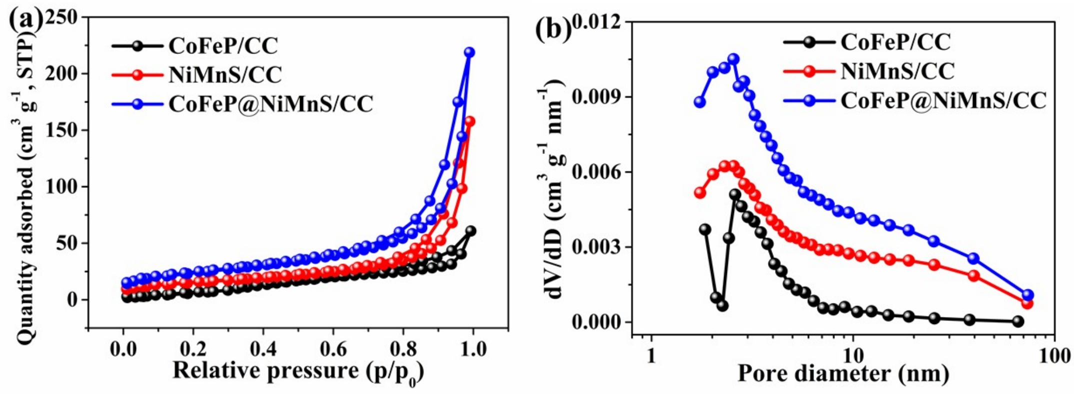


Fig. S3 (a) $N_2$ adsorption-desorption isotherms, and (b) pore size distributions of the CoFeP/CC, NiMnS/CC, and CoFeP@NiMnS/CC.

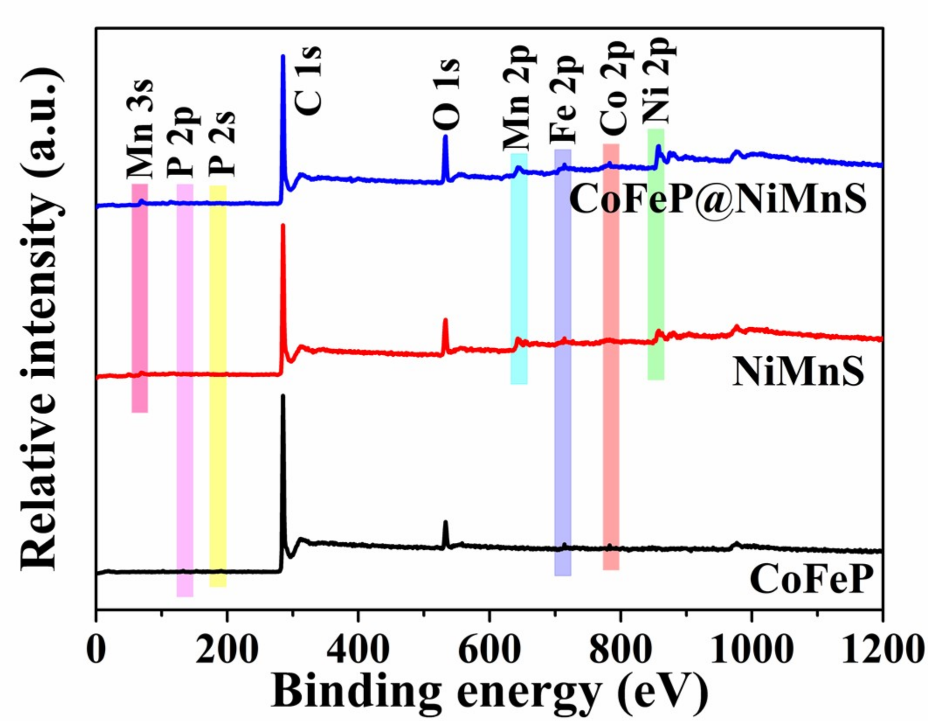


Fig. S4 XPS surveys of CoFeP/CC, NiMnS/CC, and CoFeP@NiMnS/CC.

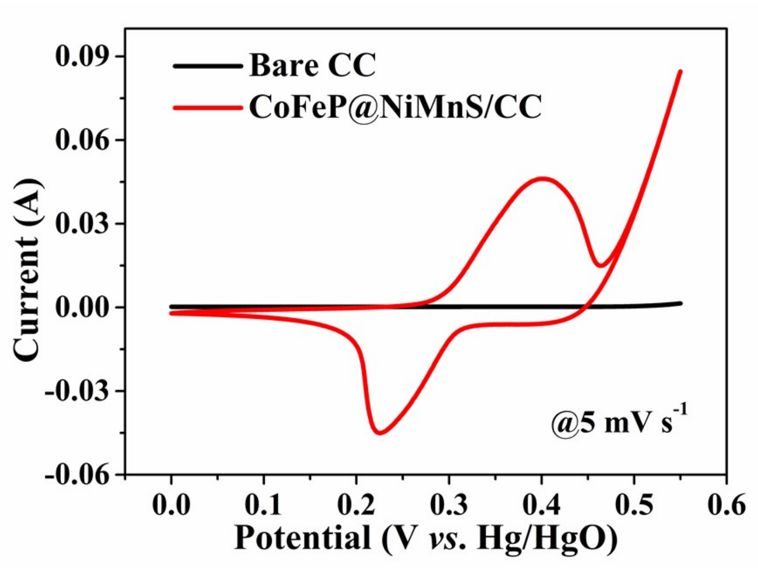


Fig. S5 Comparison of CV curves of bare carbon cloth and CoFeP@NiMnS/CC electrodes at a scan rate of 5 mV $s^{-1}$.

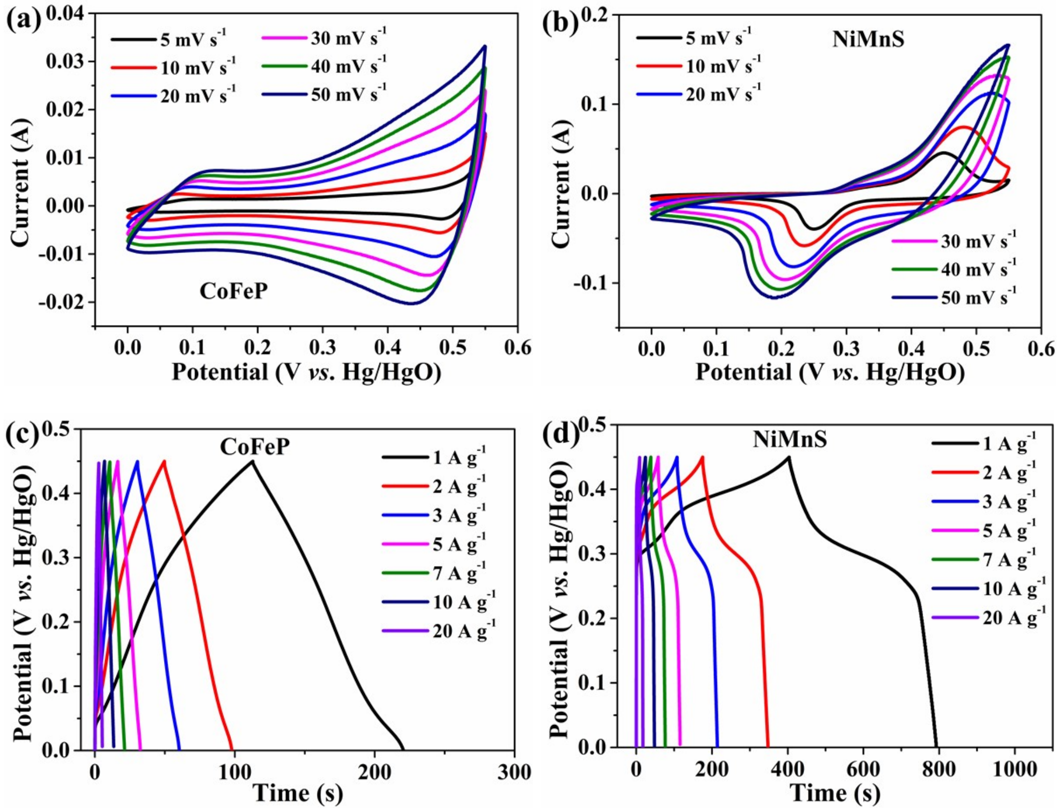


Fig. S6 Electrochemical performance tested in a three-electrode system in 2.0 M KOH electrolyte: CV curves of (a) CoFeP/CC electrode and (b) NiMnS/CC electrode, and GCD curves of (c) CoFeP/CC electrode and (d) NiMnS/CC electrode.

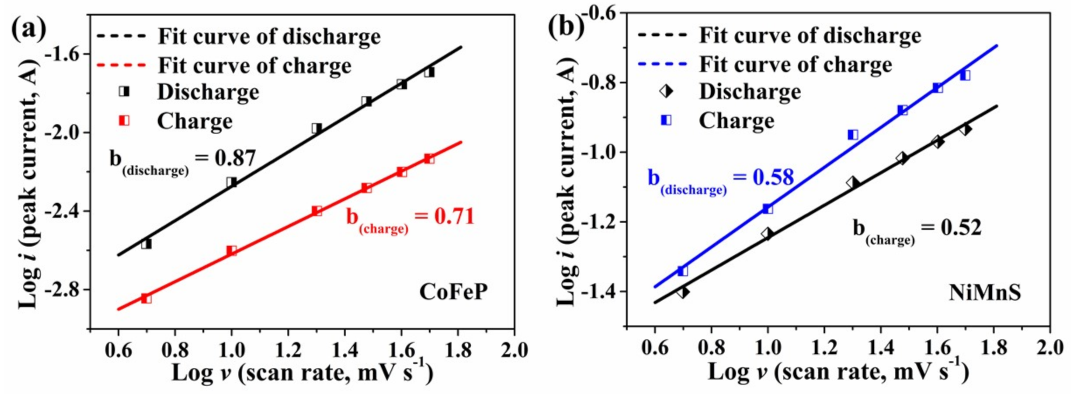


Fig. S7 The linear relationship between the peak current and the scan rate during charge and discharge for (a) the CoFeP/CC and (b) NiMnS/CC electrodes.

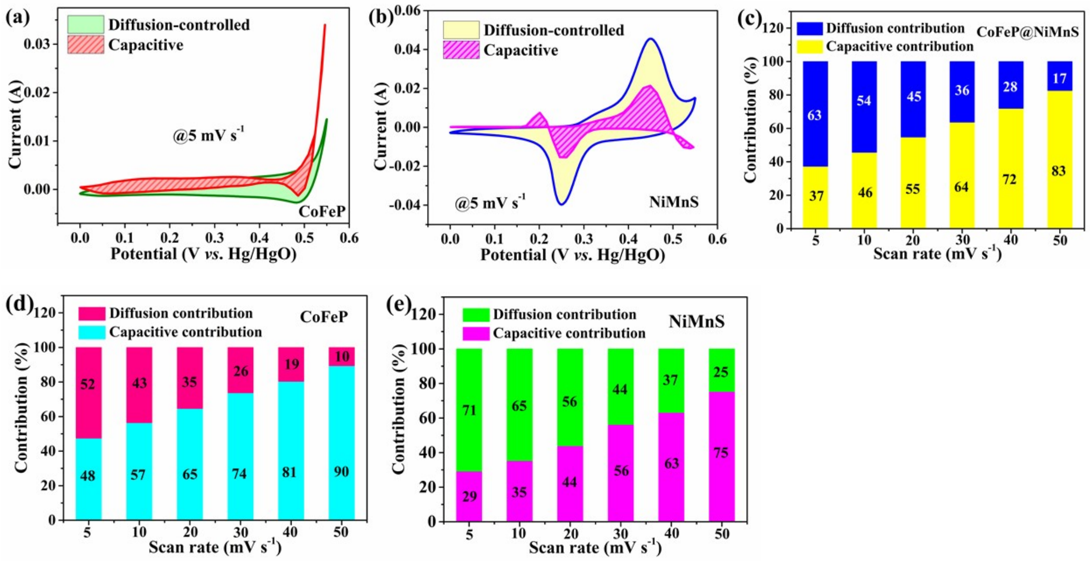


Fig. S8 The diffusion-controlled and capacitive-controlled CV response at 5 mV $s^{-1}$ of (a) the CoFeP/CC and (b) NiMnS/CC electrode, and the percentages of capacitive contribution at different scan rates of 5-50 mV $s^{-1}$ for (c) CoFeP@NiMnS/CC, (d) CoFeP/CC, and (e) NiMnS/CC electrodes.

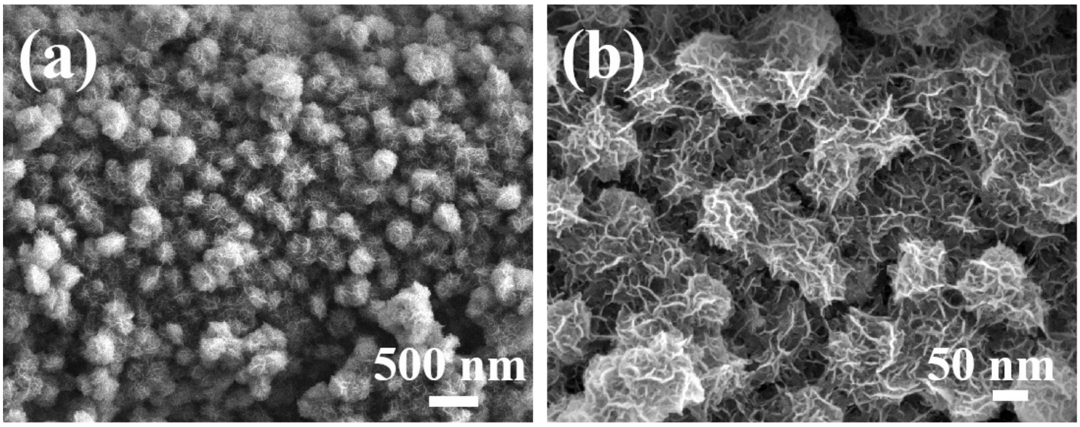


Fig. S9 SEM images of CoFeP@NiMnS/CC electrode after 5000 cycles at 5 A $g^{-1}$ at (a) low and (b) high magnifications.

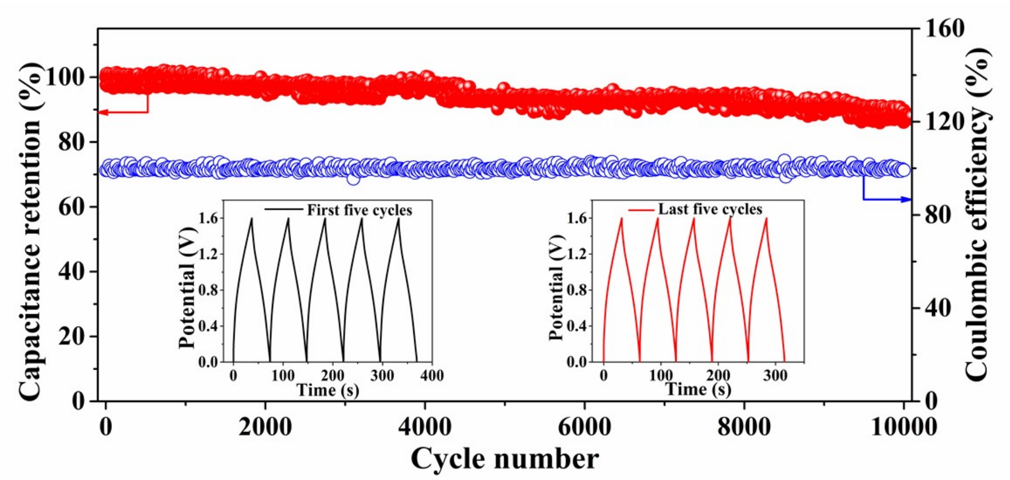


Fig. S10 The cyclic performance and coulombic efficiency of the assembled CoFeP@NiMnS/CC//LPC-Cu HSC device over 10000 cycles at 5 A $g^{-1}$ (inset shows the first and last five GCD cycles).

**Table S1** Specific surface areas and pore parameters of CoFeP/CC, NiMnS/CC, and CoFeP@NiMnS/CC.

| Samples | $S_{BET}$ ($m^2$ $g^{-1}$)[a] | $S_{micro}$ ($m^2$ $g^{-1}$)[b] | $V_{total}$ ($cm^3$ $g^{-1}$)[c] | $V_{micro}$ ($cm^3$ $g^{-1}$) |
|---|---|---|---|---|
| CoFeP/CC | 38.6 | 1.02 | 0.102 | 0.008 |
| NiMnS/CC | 61.3 | 4.73 | 0.137 | 0.031 |
| CoFeP@NiMnS/CC | 89.7 | 6.36 | 0.169 | 0.082 |

[a] Specific surface area ($S_{BET}$) was calculated via Brunauer-Emmett-Teller (BET) method.

[b] Micropore surface area ($S_{mic}$) was calculated from t-plot method.

[c] Total pore volume ($V_{total}$) was obtained from the adsorbed amount at a relative pressure of 0.99.

**Table S2** Comparison of the electrochemical performances of the as-fabricated CoFeP@NiMnS/CC electrode with previously reported core-shell electrode materials in literature.

| Electrode | Synthesis method | Specific capacity (mAh $g^{-1}$) | Rate performance | Maximum energy density (W $kg^{-1}$) | Cycling stability | Ref. |
|---|---|---|---|---|---|---|
| NiCoP@CoS | Hydrothermal method and phosphorization | 1796 F $g^{-1}$ (2 A $g^{-1}$) | 68.3% (20 A $g^{-1}$) | 35.8 Wh $kg^{-1}$ at 748.9 W $kg^{-1}$ | 86.1% after 10000 cycles | 1 |
| NiCoP@$MoSe_2$ | Hydrothermal, phosphorization and CVD | 2245.4 F $g^{-1}$ (1 mA $cm^{-2}$) | 91.6% (10 A $g^{-1}$) | 55.1 Wh $kg^{-1}$ at 799.8 W $kg^{-1}$ | 95.8% after 8000 cycles | 2 |
| CoP@NiCoP | Hydrothermal method and phosphorization | 265.5 (2 A $g^{-1}$) | 61.68% (25 A $g^{-1}$) | 37.16 Wh $kg^{-1}$ at 875 W $kg^{-1}$ | 50% after 1000 cycles | 3 |
| NiCoP/NiCo-OH | Hydrothermal method and phosphorization | 1100 (1 A $g^{-1}$) | 60% (10 A $g^{-1}$) | 34 Wh $kg^{-1}$ at 775 W $kg^{-1}$ | 92% after 1000 cycles | 4 |
| CuCo-P@ $Ni(OH)_2$ | Solvotherma,phosphorization and electrodeposition | 230.6 (2 mA $cm^{-2}$) | 86.3% (20 mA $cm^{-2}$) | 40 Wh $kg^{-1}$ at 319.6 W $kg^{-1}$ | 73% after 6000 cycles | 5 |
| $ZnCo_2O_4$@ Ni-Co-S | Hydrothermal method and electrodeposition | 1396.9 C $g^{-1}$ (1 A $g^{-1}$) | 52.8% (10 A $g^{-1}$) | 53.1 Wh $kg^{-1}$ at 3375 W $kg^{-1}$ | 85.5% after 10000 cycles | 6 |
| Co-CH@NiCoMn-CH | Solvothermal method | 3224 F $g^{-1}$ (1 A $g^{-1}$) | 83.97% (5 A $g^{-1}$) | 20.31 Wh $kg^{-1}$ at 748.46 W $kg^{-1}$ | 90.4% after 6000 cycles | 7 |
| Co-$MoS_2$@ $Cu_2MoS_4$ | Hydrothermal method | 220 (1 A $g^{-1}$) | 64% (10 A $g^{-1}$) | 41.6 Wh $kg^{-1}$ at 6240 W $kg^{-1}$ | 92.8% after 5000 cycles | 8 |
| **CoFeP@ NiMnS/CC** | **Hydrothermal, phosphorization and electrodeposition** | **260.7 (1 A $g^{-1}$)** | **65.9% (20 A $g^{-1}$)** | **60.1 Wh $kg^{-1}$ at 371.8 W $kg^{-1}$** | **85.7% after 10000 cycles** | **This work** |

## References


[1] Z. Xu, C. Du, H. Yang, J. Huang, X. Zhang, J. Chen, NiCoP@CoS tree-like core-shell nanoarrays on nickel foam as battery-type electrodes for supercapacitors, Chem.

Eng. J. (2021) 127871.

[2] X. Gao, L. Yin, L. Zhang, Y. Zhao, B. Zhang, Decoration of NiCoP nanowires with interlayer-expanded few-layer $MoSe_2$ nanosheets: A novel electrode material for asymmetric supercapacitors, Chem. Eng. J. 395 (2020) 125058.

[3] X. Wang, C. Jing, W. Zhang, X. Wang, X. Liu, B. Dong, Y. Zhang, One-step phosphorization synthesis of CoP@NiCoP nanowire/nanosheet composites hybrid arrays on Ni foam for high performance supercapacitors, Appl. Surf. Sci. 532 (2020) 147437.

[4] X. Li, H. Wu, A.M. Elshahawy, L. Wang, S.J. Pennycook, C. Guan, J. Wang, Cactus-like NiCoP/NiCo-OH 3D architecture with tunable composition for high-performance electrochemical capacitors, Adv. Funct. Mater. 28 (2018) 1800036.

[5] X. Li, J. Huang, L. Wang, J. Zhang, S. Song, G. Li, P. Wang, P. Sun, Y. Yang, Hierarchical honeycomb-like networks of CuCo-P@$Ni(OH)_2$ nanosheet arrays enabling high-performance hybrid supercapacitors, J. Alloys Compd. 838 (2020) 155626.

[6] M. Dai, D. Zhao, H. Liu, X. Zhu, X. Wu, B. Wang, Nanohybridization of Ni-Co-S nanosheets with $ZnCo_2O_4$ nanowires as supercapacitor electrodes with long cycling stabilities, ACS Appl. Energy Mater. 4 (2021) 2637−2643.

[7] Y. Zhong, X. Cao, Y. Liu, L. Cui, J. Liu, Nickel cobalt manganese ternary carbonate hydroxide nanoflakes branched on cobalt carbonate hydroxide nanowire arrays as novel electrode material for supercapacitors with outstanding performance, J. Colloid Interf. Sci. 581 (2021) 11−20.

[8] S.K. Hussain, B.N.V. Krishna, G. Nagaraju, S.C. Sekhar, D. Narsimulu, J.S. Yu, Porous Co-$MoS_2$@$Cu_2MoS_4$ three-dimensional nanoflowers via in situ sulfurization of $Cu_2O$ nanospheres for electrochemical hybrid capacitors, Chem. Eng. J. 403 (2021) 126319.